Unstable Whistler-Wave Propagation along the Resonance Cone in a Large Beam-Plasma System*

R. L. Stenzel†
TRW Systems, Redondo Beach, California 90278
(Received 26 July 1976)

A very-large-diameter ($\sim \frac{1}{2}$ m) uniform electron beam is injected along a magnetic field ($B_0 \simeq 75$ G) into a dense background plasma ($n_e \simeq 10^{10}$ cm^{-3}). The beam drives oblique whistler waves ($\omega < \omega_c < \omega_p$) unstable which are in resonance with the beam ($\omega/k_\parallel \simeq v_b$) and propagate nearly along the resonance cone angle ($\cos\theta = k_\parallel/k \simeq \omega/\omega_c$). Growth of test waves as well as spontaneous broad-band emission reminiscent of very-low-frequency hiss are observed.

There is considerable interest in the properties of oblique whistler waves, in particular, near the lower-hybrid frequency and for propagation directions along the resonance cone. While linear- and nonlinear-wave experiments have been reported,[1-3] the interaction of oblique whistlers with electron beams has not yet been studied experimentally. Related observations of very-low-frequency (VLF) hiss in space plasmas[4] and lower-hybrid emission in tokamaks[5] indicate the existence of beam-plasma instabilities. This Letter presents the first observations of convective amplification of whistler waves along the resonance cone in a large laboratory plasma. An electrostatic beam-plasma instability arises when the beam velocity matches the parallel phase velocity of an oblique whistler ($v_b \gtrsim \omega/k_\parallel$).[6] The propagation angle $\theta = \arctan(k_\perp/k_\parallel)$ is determined by the whistler dispersion relation.[7] For slow beams ($v_b \ll c\omega_p/\omega_c$), θ is close to the phase-velocity resonance cone angle $\theta \simeq \arccos(\omega/\omega_c)$ and the wave number is given by $k = \omega_c/v_b$.[8] The instability can occur at any frequency between the lower hybrid and the electron cyclotron resonance. Wave amplification takes place along the group-velocity resonance cone of angle $\theta_c \simeq \arcsin(\omega/\omega_c)$.

In contrast to the typical small-diameter beam-plasma experiments,[9-11] the present experiment is performed with an electron beam of diameter D large compared to the instability wavelength ($k_\perp D \simeq 100$). Amplification of test waves and spontaneous noise emission within this nearly unbounded beam-plasma system are observed. The experimental setup shown in Fig. 1(a) employs a solid oxide-coated cathode of diameter $D \simeq \frac{1}{2}$ m which, in a pulsed mode [see Fig. 1(b)], produces a uniform, quiescent, magnetized afterglow plasma (with $n_e = 10^9$–10^{11} cm^{-3}, $kT_e \simeq 0.3$ eV, and $B_0 = 75$ G) into which a cold electron beam (with $V_b \simeq 40$ V, $kT_b \lesssim 1$ eV, and $n_b = 10^8$–10^9 cm^{-3}) is injected [see Fig. 1(c)]. Beam and plasma properties are diagnosed with probes and rf techniques. Movable, coaxially fed, short-wire rf probes are used to excite and/or detect whistler waves. Narrow-band interferometer techniques yield the spatial wave properties; sampling techniques are used to obtain temporally resolved data.

The propagation of test whistler waves in the beam-plasma system is summarized in Fig. 2. The waves are launched from one of the rf probes located at the origin of Figs. 2(c) and 2(d). In the absence of beams, a point rf exciter exhibits

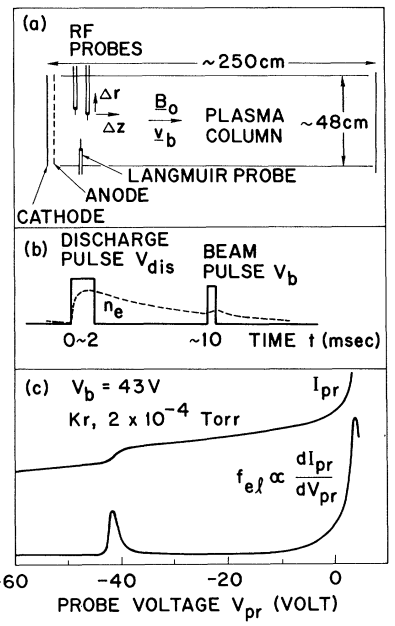

FIG. 1. (a) Schematic view of experimental setup. (b) Typical time sequence for injecting a pulsed electron beam into a cold Maxwellian afterglow plasma. (c) Measured probe characteristic (top trace) and derived electron distribution function (bottom trace) sampled at $t_s = 25$ μsec after turn-on of the beam pulse applied at $t_a = 15$ msec in the afterglow ($n_e \simeq 7 \times 10^9$ cm^{-3}, $n_b/n_e \simeq 3\%$). Probe position $z \simeq 8$ cm from cathode.

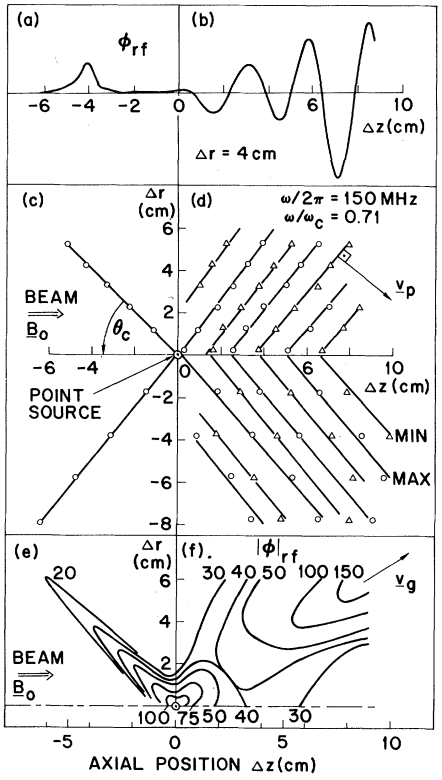

FIG. 2. Properties of small-amplitude test waves excited from a point source in a beam-plasma system. (a), (b) An axial interferometer trace shows a highly localized field for propagation against the beam but growing waves for propagation with the beam. A two-dimensional phase-front map shows (c) a resonance cone pattern against the beam and (d) oblique waves with the beam. A contour map of constant rf amplitudes (arbitrary units) shows (e) amplitude decay along the diverging cone opposing the beam but (f) oblique amplitude growth with the beam. Note that for the unstable mode $\omega/k_{\parallel} \simeq v_b$ and $\vec{v}_g \sim \perp \vec{v}_p$. Parameters: $\omega_p/\omega_c \simeq 3$, $t_s = 10$ μsec, $V_b \simeq 38$ V.

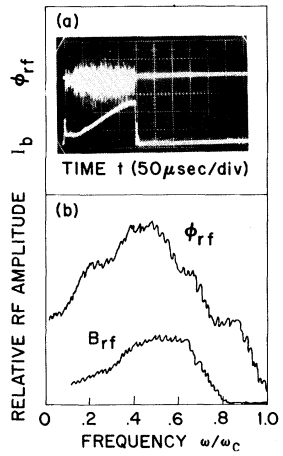

FIG. 3. (a) Top trace: Noise emission at $\omega/\omega_c = 0.47$ (heterodyned with $f_{l0} = 100$ MHz). Bottom trace: Beam current pulse (40 A/div, $V_b \simeq 40$ V) vs time. Afterglow time $t_a = 10$ msec. (b) Frequency spectrum sampled at $t_s = 100$ μsec after turn-on of the beam pulse. φ_{rf} is the electrostatic rf potential detected in the instability region; B_{rf} is the wave magnetic field of the unstable whistlers detected 125 cm away from the excitation region. $\omega_c/2\pi = 210$ MHz, $\omega_p/\omega_c \simeq 6$.

a radiation pattern in the form of two symmetric resonance cones with axis along $\vec{B}_0$, apex at the exciter, and cone half-angle $\theta_c \simeq \arcsin(\omega/\omega_c)$ when $\omega_c^2 \ll \omega_p^2$.[1] The presence of an electron beam strongly changes the radiation properties in the direction of the beam but not in the opposite direction. Axial interferometer traces shown in Figs. 2(a) and 2(b) exhibit a highly localized rf potential in the half space opposing $\vec{v}_b$ and growing waves in the opposite direction. A map of the phase fronts in the r-z [Figs. 2(c) and 2(d)] reveals that, under the reasonable assumption of azimuthal symmetry, the radiation opposing $\vec{v}_b$ is along the group-velocity resonance cone [$\theta_c \simeq \arcsin(\omega/\omega_c) \simeq 45°$]; but with $\vec{v}_b$, a well-defined wave with conical phase surfaces is excited. The parallel phase velocity matches the beam velocity (i.e., $f\lambda_{\parallel} \simeq v_b \simeq 3.6\times10^8$ cm/sec) and the wave normal angle with respect to $\vec{B}_0$ is close to that for oblique resonance, $\theta \simeq \arccos(\omega/\omega_c) \simeq 45°$. The relative amplitude distribution is displayed in Figs. 2(e) and 2(f) as a contour map in the quadrants above the symmetry axis $\Delta r = 0$. Along the resonance cone opposing the beam, the amplitude decays because of the divergence of the energy flow; but with the beam, amplitude growth is observed. The direction of maximum growth, i.e., the group-velocity direction, is essentially perpendicular to that of the phase velocity ($\vec{v}_g \sim \perp \vec{v}_p$), which is characteristic for the resonance cone mode.[1-3] The growth length, $k_i^{-1} \simeq 4$ cm, is much smaller than the beam dimensions along $\vec{v}_g$. Thus, there is sufficient convective growth in the system to observe the instability being spontaneously excited from thermal noise. These observations are described below.

Figure 3(a) shows the spontaneous emission of whistler waves (top trace, $\omega/\omega_c = 0.47$) due to the injection of the pulsed electron beam (bottom trace) into a quiescent background plasma. Figure 3(b) displays frequency spectra sampled at $t_s = 100$ μsec after turn-on of the beam for both an electrostatic probe signal φ_{rf} near the beam-injection region ($z \simeq 8$ cm from cathode) and a

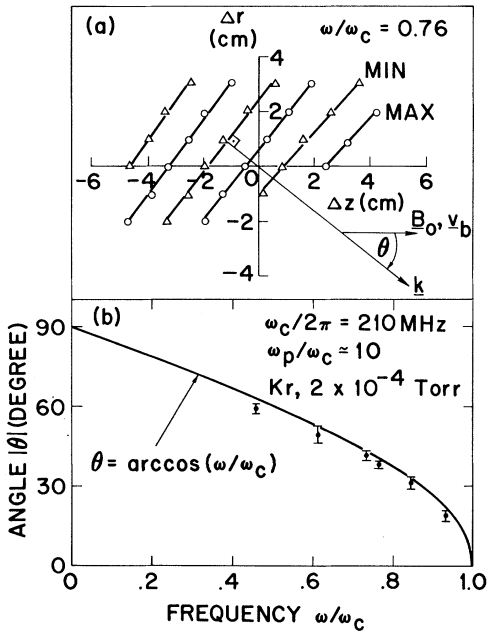

FIG. 4. (a) Phase fronts (minima and maxima of narrow-band cross-correlation signal) of unstable oblique whistlers sampled at $t_s = 30$ μsec after turn-on of beam pulse ($v_b \simeq 4\times10^8$ cm/sec). The direction of the propagation vector k is obtained from phase shift measurements. The fixed reference probe at $\Delta r = \Delta z = 0$ is located 8 cm away from cathode. (b) Angle of wave propagation vs frequency. Solid line: oblique resonance condition ($k \to \infty$).

magnetic-loop signal B_{rf} at larger distances from the cathode ($z \simeq 125$ cm). rf emission is observed at essentially all whistler-wave frequencies between the lower hybrid and the electron cyclotron resonance. There are also higher-frequency components, in particular near $\omega = \omega_p$, but these will be considered elsewhere.

The absolute wave amplitudes are estimated in two different ways. First, from the transmission loss between two electrostatic probes the wave-probe coupling factor is obtained[12] which yields normalized rf potentials $e\varphi_{rf}/kT_e \simeq 5\times10^{-3}$ (where $kT_e/e \simeq 1.5$ eV in the presence of the beam). Second, by calibrating the magnetic-loop antenna[3] the absolute wave magnetic field is obtained ($B_{rf}/B_0 \simeq 10^{-5}$) from which the wave electric field can be calculated.[7] The wave intensities are, in general, smaller than those encountered in narrow-band instabilities[9-11] such that secondary nonlinear effects like parametric instabilities or trapped-particle effects may not play an important role.

The spatial properties of the emitted waves are obtained from narrow-band correlation measurements with two rf probes, one of which is movable in the radial and axial directions. Figure 4(a) shows the phase fronts of a particular frequency component ($\omega/\omega_c = 0.76$). The parallel phase velocity essentially matches the beam velocity ($\omega/k_\parallel \simeq v_b$). The wave propagation is oblique to the beam; and the angle θ between the propagation vector $\vec{k}$ (normal to phase front) and the static magnetic field $\vec{B}_0$ is below but close to that for the oblique-resonance condition in a dense plasma, $\theta = \arccos(\omega/\omega_c)$. Corresponding measurements at other frequencies [see Fig. 4(b)] show that θ varies with frequency as predicted by theory. Thus, just like the unstable test waves, the spontaneously emitted rf noise consists of unstable whistlers propagating along the resonance cone. However, since the spatial origin of the rf emission is not as well defined as for the test waves, the observed phase fronts show considerable variations. At some frequencies, the k vector points radially inward, at others outward, and occasionally both are superimposed. Thus, the results shown in Fig. 4(b) refer to the magnitude of θ_{max}. It is also worth pointing out that low-frequency components are found to be well correlated along $\vec{B}_0$ while high frequencies ($\omega \lesssim \omega_c$) correlate better across $\vec{B}_0$, consistent with the fact that amplification is along $\vec{v}_g$ and $\vec{v}_g \sim \perp \vec{v}_p$.

In summary, amplification of whistler waves propagating along the resonance cone in a nearly unbounded beam-plasma system has been observed. It should be pointed out that present models of auroral VLF hiss[13] are based on the same instability and that these laboratory observations basically confirm the proposed generation mechanism for broad-band whistler waves. Detailed results will be published elsewhere.[14]

The author acknowledges helpful discussions with R. W. Fredricks and J. Maggs, and technical assistance from W. F. Daley.

*Work supported by TRW Internal Research and Development funds.

†Also Department of Physics, University of California, Los Angeles, Calif. 90024.

[1]R. K. Fisher and R. W. Gould, Phys. Fluids 14, 857 (1971).

[2]R. J. Briggs and R. R. Parker, Phys. Rev. Lett. 29, 852 (1972).

[3]R. L. Stenzel, Phys. Fluids 19, 857 (1976); R. L. Stenzel and W. Gekelman, to be published, and Phys.

Rev. A 11, 2057 (1975).

[4]D. A. Gurnett and L. A. Frank, J. Geophys. Res. 77, 172 (1972).

[5]B. Coppi, F. Pegoraro, R. Pozzoli, and G. Rewoldt, Nucl. Fusion 16, 309 (1976).

[6]A. B. Mikhailovskii, *Theory of Plasma Instabilities* (Consultants Bureau, New York, 1974), Vol. 1, Chap. 9.

[7]R. A. Helliwell, *Whistlers and Related Ionospheric Phenomena* (Stanford Univ. Press, Stanford, Calif., 1965), Chap. 3.

[8]Wave amplification oblique to a beam also occurs for ion acoustic waves driven unstable by an ion beam. [See, for example, T. Ohnuma, T. Fujita, and S. Adachi, Phys. Rev. Lett. 36, 471 (1976)]. It is interesting to note that because of the different dispersion relation the wave number k is determined by the dispersion $\omega = kc_s$, and the propagation angle $\theta = \arccos(v_b/c_s)$ is given by the beam velocity, whereas the opposite holds for the whistler waves. P. Bellan, private communication.

[9]J. H. Malmberg and C. B. Wharton, Phys. Fluids 12, 2600 (1969).

[10]L. D. Bollinger, W. Carr, H. Liu, and M. Seidl, Phys. Fluids 17, 2142 (1974).

[11]K. W. Gentle and J. Lohr, Phys. Fluids 16, 1464 (1973).

[12]J. H. Malmberg and C. B. Wharton, Phys. Rev. Lett. 19, 775 (1967).

[13]D. W. Swift and J. R.Kan, J. Geophys. Res. 80, 785 (1975); J. Maggs, J. Geophys. Res. 81, 1707 (1976).

[14]R. Stenzel, to be published.

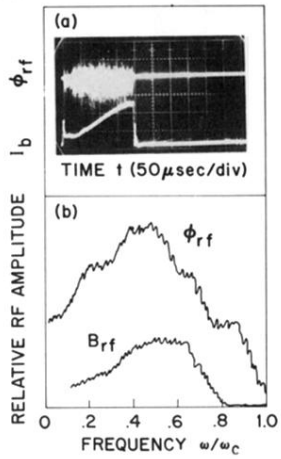

FIG. 3. (a) Top trace: Noise emission at $\omega/\omega_c = 0.47$ (heterodyned with $f_{I0} = 100$ MHz). Bottom trace: Beam current pulse (40 A/div, $V_b \simeq 40$ V) vs time. Afterglow time $t_a = 10$ msec. (b) Frequency spectrum sampled at $t_s = 100$ μsec after turn-on of the beam pulse. φ_{rf} is the electrostatic rf potential detected in the instability region; B_{rf} is the wave magnetic field of the unstable whistlers detected 125 cm away from the excitation region. $\omega_c/2\pi = 210$ MHz, $\omega_p/\omega_c \simeq 6$.